Highly Crystalline Methylammonium Lead Tribromide Perovskite Films for Efficient Photovoltaic Devices

Nakita K. Noel,[1,2*] Bernard Wenger,[1] Severin N. Habisreutinger,[1,3] Jay B. Patel,[1] Timothy Crothers,[1] Zhiping Wang,[1] Robin J. Nicholas,[1] Michael B. Johnston,[1] Laura M. Herz,[1] Henry J. Snaith[1*]

[1] Clarendon Laboratory, Department of Physics, University of Oxford, Parks Road, Oxford, UK, OX1 3PU

[2] Department of Electrical Engineering, Princeton University, Olden Street, NJ, 08544, USA

[3] National Renewable Energy Laboratory, 15013 Denver West Parkway, Golden, USA

Corresponding Authors: henry.snaith@physics.ox.ac.uk; nnoel@princeton.edu

Abstract:

The rise of metal-halide perovskite solar cells has captivated the interest of the research community, promising to disrupt the current energy landscape. While a sizable percentage of the research done on this class of materials has been focused on the neat, and iodide-rich perovskites, bromide-based perovskites can deliver substantially higher voltages due to their relatively wide bandgaps of over 2 eV. The potential for efficient, high-voltage devices makes materials such as these incredibly attractive for multi-junction PV applications. In this work we use the acetonitrile/methylamine solvent system to deposit smooth, highly crystalline films of $CH_3NH_3PbBr_3$. By using choline chloride as a passivating agent for these films, we achieve photoluminescence quantum efficiencies of up to 5.5%, and demonstrate charge-carrier mobilities of 17.8 cm^2/Vs. Incorporating these films into photovoltaic devices, we achieve scanned power conversion efficiencies of up to 8.9%, with stabilized efficiencies of 7.6%, providing a simple way forward to realize efficient, high-voltage $CH_3NH_3PbBr_3$ planar-heterojunction devices.

Introduction:

Metal halide perovskites have amassed tremendous interest over the last five years, largely due to the impressive power conversion efficiencies (PCE) that have been achieved with perovskite based solar cells.[1, 2] In a relatively short period of time, the PCEs of lead halide perovskite solar cells have soared from 3.8%[3] to a certified 22.1%.[4] This rapid increase in PCE can largely be attributed to the development and application of improved deposition techniques, as well as careful tuning of the perovskite composition and stoichiometry.

Most of the research effort has been focused on the methylammonium lead triiodide ($CH_3NH_3PbI_3$) and formamidinium lead triiodide ($HC(NH_2)_2PbI_3$), or iodide rich, mixed cation and mixed halide perovskites. Indeed, the highest efficiency perovskite solar cells utilize the more thermally stable $HC(NH_2)_2PbI_3$ with inclusions of small amounts of Cs^+, Br^- and $CH_3NH_3^+$ to provide structural stability, and to further increase the thermal stability of the material.[5-7] Comparatively little effort has been placed on the development of the neat bromide, and bromide rich compositions of lead based perovskites, likely due to their larger bandgaps which are less ideal for high efficiency single-junction solar cells. While the neat iodide and the iodide rich compositions of lead based perovskites are very close to ideal for single junction solar cells, the wider bandgap bromide based perovskites (E_g > 2.0 eV) are promising candidates for implementation in perovskite-based tandem, and triple junction solar cells.[8]

A metric with which to assess the fundamental energy loss is a photovoltaic device, is to estimate the difference in energy between the band gap of the absorber layer (the lowest energy at which photons are absorbed) and the open-circuit voltage (V_{OC}) which the solar cell generates under full sun-light. In an ideal solar cell this “loss-in-potential” or “voltage deficit” is in the range of 300 mV. While the band gap of the $HC(NH_2)_2PbBr_3$ and $CH_3NH_3PbBr_3$ perovskites are approximately 2.2 eV to 2.3 eV, the highest voltage which has been reported for these systems is 1.61 V.[9] This makes the loss-in-potential for the neat bromide perovskite devices > 600 mV, which is almost twice as large as the 360 mV achieved for the iodine rich perovskite cells.[10-12] A variety of reasons for this increased voltage have been postulated, one of which is an unfavourable alignment between the highest molecular orbital (HOMO) of the more commonly used hole transporting materials such as spiro-OMeTAD.[13] In some of the early work on $CH_3NH_3PbBr_3$ solar cells, efficient devices were obtained by using the triarylamine polymer derivative (PIF8-TAA) in place of spiro-OMeTAD in the conventional n-i-p configuration.[13] This was done using both mesoporous and planar TiO_2 resulting in PCEs of 6.7%[13] and 10.4%[14] respectively, with corresponding open-circuit voltages of 1.4 V and 1.51 V.

More recently, $CH_3NH_3PbBr_3$ has been employed in the p-i-n device configuration, and the same approach has been applied to the electron extraction layers (ETLs).[9, 15] Indene-C_{60} bisadduct (ICBA) possesses a lowest unoccupied molecular orbital (LUMO) level closer to vacuum than phenyl-C_{61}-butyric acid methyl ester (PCBM), a member of the family of fullerene derivatives which is widely used in the fabrication of perovskite solar cells. By replacing PCBM with ICBA in the p-i-n cell structure, Wu et al. have reported a record high voltage of 1.61 V for methylammonium lead bromide-based solar cells. This increase in voltage has been attributed to a combination of both the better positioned LUMO of ICBA, as well as it passivating the grain boundaries in the perovskite film.[9]

The rapid crystallization of the bromide-based perovskites makes it non-trivial to obtain high-quality, smooth, pinhole free films.[10, 11] While a great deal of research has been focused on improving the quality of the lead iodide based perovskite films,[16-19] comparatively little effort has been placed on improving the quality of the lead bromide based films. Most of the early work done on bromide based solar cells was either done on mesoporous films which allowed for incomplete coverage,[10, 11, 13] or were directly tailored to improving the crystallization of films, thus controlling the extent of the available shunting pathways.[11, 14, 20] Efficient, planar heterojunction bromide devices have also been fabricated using a two-step deposition method[9, 20, 21] as well as the solvent quenching approach.[15] We have recently developed a solvent system which allows for the deposition of high quality, uniform, pin-hole free $CH_3NH_3PbI_3$ films.[19] In this work, we extend the use of this solvent system to the $CH_3NH_3PbBr_3$ perovskite, and find that it produces highly crystalline films with complete coverage, as well as efficient planar heterojunction solar cells with efficiencies of over 7%, with a maximum open-circuit voltage of 1.52 V.

Results and Discussion:

We have recently shown that amines can be used in conjunction with polar, aprotic solvents such as acetonitrile (ACN) to facilitate the dissolution of $CH_3NH_3PbI_3$ perovskite precursor salts. Using a similar process here, we disperse $CH_3NH_3PbBr_3$ precursor salts in ACN and saturate the solution with methylamine (MA) gas, resulting in the dissolution of the precursor salts to obtain a clear, colourless solution (See experimental details). Upon spin-coating this solution, we obtain a smooth, dense film which has the characteristic orange colour of $CH_3NH_3PbBr_3$. While films of $CH_3NH_3PbBr_3$ are known to crystallize very rapidly from more conventional solvents such as N,N-Dimethylformamide (DMF), this rapid crystallization often comes at the expense of film quality. For DMF there usually exist many highly oriented, large crystals randomly distributed over the substrate, resulting in a high density of pinholes in the film.[11, 14] It has previously been reported that by adding hydrobromic acid (HBr) to the solution, the crystallization kinetics are changed, such that a smooth, dense film with uniform coverage can be obtained.[14] In **Figure S1** we show microscope images of films which we have obtained from both neat DMF and DMF with the addition of HBr. Here, we see that without the addition of the acid, there are large, individual crystalline domains on the substrate. When the acid is added to the DMF, these crystals become smaller and appear to be more highly oriented. However, even at the high concentration of 100 µL/mL, we are unable to achieve a uniform film with complete substrate coverage. In contrast, when deposited from the ACN/MA compound solvent, we find that the resulting film comprises what appears to be large, flat grains which fully impinge upon each other, and contain far fewer pinholes. We show the scanning electron microscope (SEM) images in **Figure 1**.

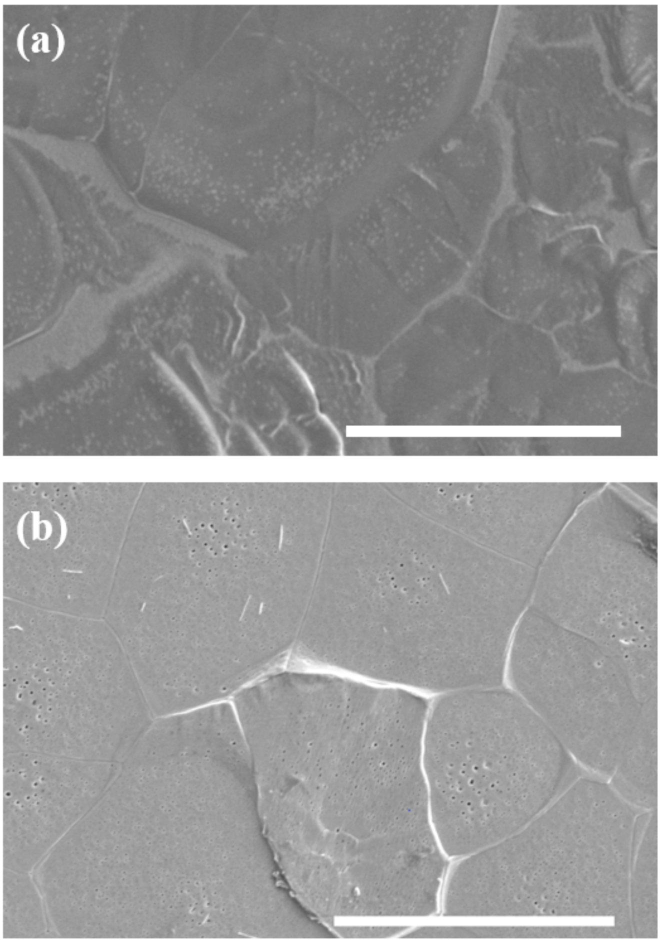

Figure 1: Microscope Images. SEM images of $CH_3NH_3PbBr_3$ deposited from (a) neat DMF and (b) the ACN/MA compound solvent. Scale bars represent a distance of 10 µm.

From the SEM images in Figure 1, it appears that films deposited from the ACN/MA solvent are not only smoother, but also maintain appreciably large grain sizes. This is in agreement with our previous observations made on the iodide-based system, that the rapid crystallization which occurs as a result of the low boiling point solvent, does not result in a loss of crystallinity in the film.[19] Interestingly, we find that the films processed from the ACN/MA solvent appear to have small holes in the crystal, which through analysis of cross sectional SEM images (which we show in

Figure S4) appear to be only on the surface of the film. While the exact cause for these is unknown, we postulate that they may be generated due to the evaporation of residual solvent which may have been trapped in the film during the rapid crystallization process. Upon heating, this solvent may evaporate causing small physical cavities in the crystals.

Next, we investigate the crystal structure and the degree of crystallinity of these films by performing X-ray diffraction (XRD) measurements. In **Figure 2** we present the results of both the powder and two-dimensional (2D) diffraction scans.

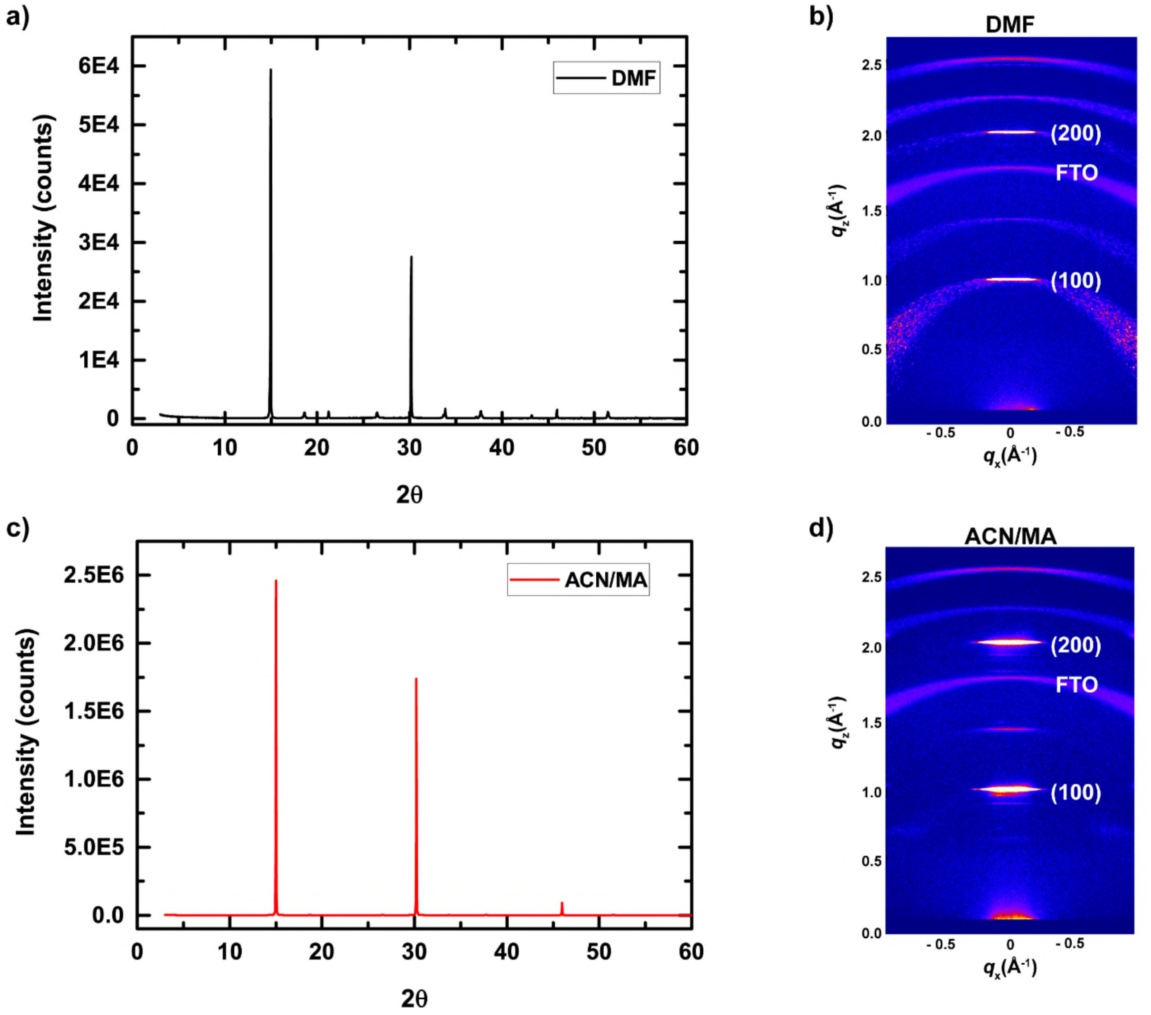

Figure 2: X-ray Diffractograms. Powder and 2D X-ray diffractograms of (a) and (b) $CH_3NH_3PbBr_3$ deposited from DMF, and (c) and (d) $CH_3NH_3PbBr_3$ deposited from ACN/MA.

In Figures 2a and 2c we show the powder diffraction patterns $CH_3NH_3PbBr_3$ films deposited from DMF and ACN/MA, respectively. For the films processed from both solvents, all the reflections can be assigned to the cubic $CH_3NH_3PbBr_3$ perovskite phase.[22] Interestingly, we see that the intensity of the (100) peak increases by approximately two orders of magnitude for the films deposited from the ACN/MA compound solvent. We note that films deposited from the two routes have very similar thicknesses (380 nm - 400 nm), and as such the differences in peak intensity cannot be attributed to a difference in film thickness. We believe that this increase in the peak intensity occurs as a result of increased texturing and grain orientation in the film deposited from the compound solvent. To gain more information on the crystallographic orientation in both these films, we performed a two-dimensional XRD (2D-XRD) measurement. The 2D hybrid pixel array detector employed in this measurement allows us to measure complete Debye-Scherrer cones.[5] We show the 2D-XRD images in Figures 2b and 2d. We observe two major reflections located at q_z = 1 and 2 Å, which correspond to the (100) and (200) reflections of the $CH_3NH_3PbBr_3$, respectively. The film deposited from DMF displays intense diffraction patterns along the specular direction. At the same time, we also notice many weak reflections across the entire arc. **Figure S2** displays the integrated (100) peak intensity in azimuthal direction (i.e. intensity vs. β). For the film deposited from DMF, we can clearly observe two broad peaks at $\beta = 120^\circ$ and $240^{\circ\circ}$ in addition to the major peak at $\beta = 180^\circ$. In contrast, for the film deposited from the ACN/MA solvent most of the (100) reflections appear in the specular direction and are distributed at $\beta = 180^\circ$ with a much higher intensity in the scattering intensity vs. β plot. This confirms that the perovskite film processed from ACN/MA solvent has a much higher degree of texture than the film deposited from DMF.

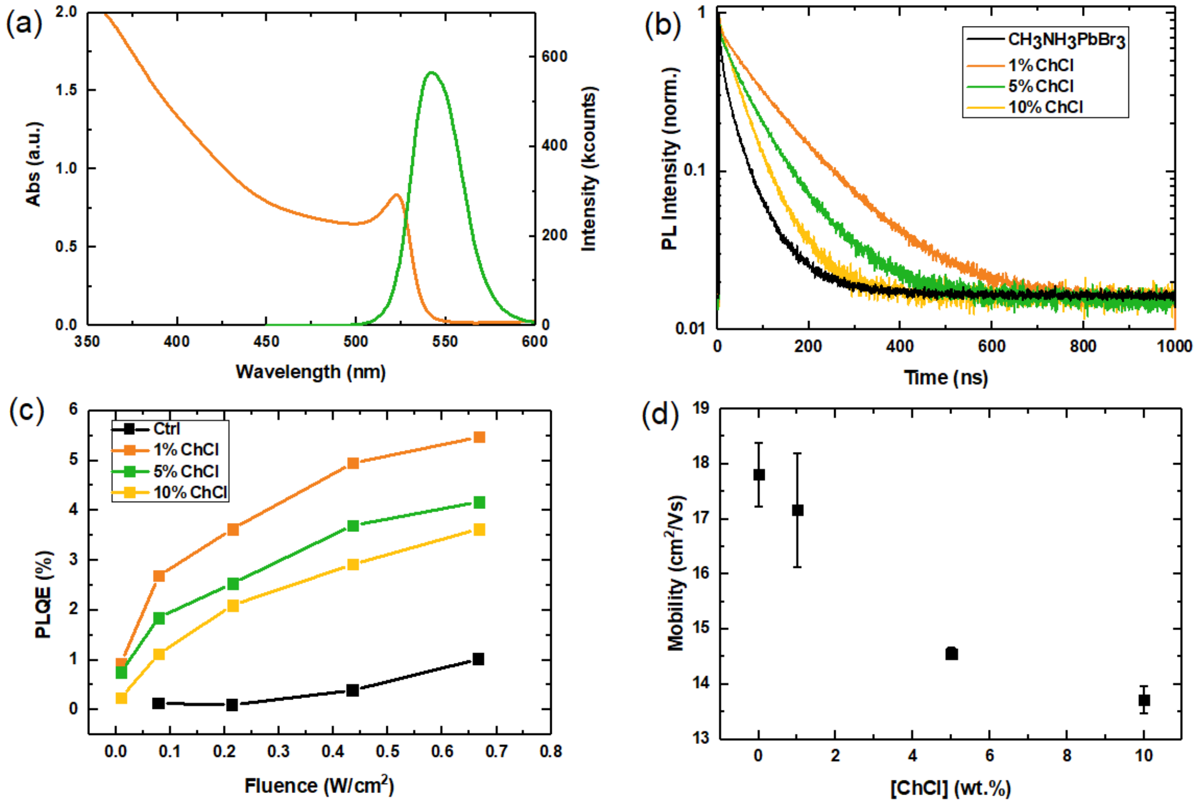

Figure 3: Optical Measurements. (a) Absorbance and steady-state photoluminescence (PL) of a thin film of $CH_3NH_3PbBr_3$. (b) PL decays of a neat $CH_3NH_3PbBr_3$ film and $CH_3NH_3PbBr_3$ films treated with choline chloride (ChCl). Film samples were photoexcited using a 405 nm laser head (LDH-P-C-510, PicoQuant GmbH) pulsed at frequencies between 0.3-10 MHz, with a pulse duration of 117ps and fluence of ~30nJ/cm^2. (c) Fluence dependent PL quantum efficiencies of neat and ChCl treated films of $CH_3NH_3PbBr_3$. (d) Charge-carrier mobilities of neat and ChCl treated films of $CH_3NH_3PbBr_3$, as measured by terahertz photoconductivity spectroscopy.

Having determined that the $CH_3NH_3PbBr_3$ films deposited from the compound solvent have both superior surface coverage and increased crystallinity, we then move on to assess the optoelectronic quality of these films through a series of optical measurements. We show the results of these investigations in **Figure 3**. In Figure 3a we show the absorbance and the PL emission of a $CH_3NH_3PbBr_3$ film. We observe the characteristic excitonic absorption onset at 540 nm, with the corresponding PL emission centred around 542 nm. Films of $CH_3NH_3PbBr_3$ have been shown to have significantly shorter PL lifetimes than their single crystal counterparts.[23, 24] While the reason for this is still largely unknown, it may be the result of defects at the grain boundaries of individual crystals which make up a polycrystalline film. Here, we attempt to passivate any defects which may be present at the grain boundaries by using a quaternary ammonium halide salt, choline chloride (ChCl). This material has recently been successfully used as a passivating agent for the mixed-cation, mixed-halide perovskite $FA_{0.83}MA_{0.17}Pb(I_{0.83}Br_{0.17})_3$.[25] Here, we carry out a post-treatment of the films with varying concentrations of ChCl (we give full experimental details in the SI). We investigate the effect of the ChCl by examining the PL decays as well as the photoluminescence quantum efficiency (PLQE) of the control and passivated $CH_3NH_3PbBr_3$ films. In general, a longer PL lifetime/higher PLQE indicates the presence of long lived carrier species and a reduction of non-radiative recombination within the film, which is one of the main loss pathways for charge carriers in optoelectronic devices. The photoluminescence decays are characterized by a very fast drop during the first tens of nanoseconds which has been attributed to either inhomogeneity within the films, and/or diffusion of carriers within the film.[24, 26] This is followed by a slower decay phase which follows a nearly mono-exponential rate. Here, we fit the longer time slow component of the decays with a monoexponential function and extract lifetimes. For the 1% ChCl treated sample, we observe a significant increase in the PL lifetime, from 47 ns for the control film to 111 ns for the 1% ChCl treated sample. However, upon further increasing the ChCl concentration, we observe a steady decrease in the PL lifetime, to 79 ns and 51 ns for the

5% ChCl and 10% ChCl treated samples respectively (see SI). For the photoluminescence quantum efficiency (PLQE), which we show in Figure 3c, we observe an increase with respect to the control, for all the ChCl treated films. Notably, we estimate a PLQE increase from 1.0% to 5.5% for the 1% ChCl treatment, suggesting that the use of this treatment does acts to inhibit non-radiative recombination processes in the $CH_3NH_3PbBr_3$ perovskite. We have recently discussed the optical properties of large single crystals of $CH_3NH_3PbBr_3$, and measured external PLQEs of up to 6.0%.[24] With the use of the ChCl surface treatment on our thin films, we find that we can achieve PLQEs approaching that of our best single crystals, indicating improved optoelectronic quality. We do concur however, that self-absorption effects more strongly limit optical out-coupling in large single crystals, indicating that the internal luminescence quantum yield of our films will still be lower than that of the single crystals. Furthermore, we observe that with increasing concentration of ChCl, there is a blue-shift in the absorption onset. This is likely to be due to the incorporation of a small fraction of the Cl^- ions into the perovskite structure.[10, 27] We show the absorption spectra of these films in **Figure S3**.

We further probe the films by use of optical-pump terahertz-probe spectroscopy to determine the charge-carrier mobility in both neat and ChCl treated $CH_3NH_3PbBr_3$ films. It has previously been shown that bromide perovskites show stronger Fröhlich coupling than their iodide counterparts, fundamentally limiting charge-carrier mobility,(cite Laura natcomms) and as such, we expect the charge-carrier mobility of the bromide-based perovskites to be significantly lower. For example, using Hall effect and resistivity measurements, hole mobilities of 40 cm^2/Vs and 105 cm^2/Vs were obtained for single crystals of $CH_3NH_3PbBr_3$ and $CH_3NH_3PbI_3$ respectively. While charge-carrier mobilities for films of the formamidinium and formamidinium-cesium bromide perovskites have previously been determined,[28, 29]to the best of our knowledge, there are no reports in which the carrier mobility in thin films of $CH_3NH_3PbBr_3$ has been directly measured. From our measurements, we determine the charge carrier mobility in the neat $CH_3NH_3PbBr_3$ film deposited from ACN/MA to be 17.8 ± 0.6 cm^2/Vs, which is slightly higher than the mobilities reported for the neat $HC(NH_2)_2PbBr_3$ perovskite (14 cm^2/Vs) processed from a DMF solvent (cite Waqaas). Interestingly, when the ChCl is deposited onto the film at a low concentration (1 wt.%), the mobility appears to be largely unchanged (17.1 ± 1.0 cm^2/Vs), however as we increase the concentration, we observe the mobility to decrease to 13.7 cm^2/Vs (Figure 3d). From the charge-carrier mobilities and the lifetimes we can estimate the diffusion lengths of the free carriers, which range between 1.3 µm (ChCl 10%) and 2.2 µm (ChCl 1%) for the treated films, and 1.5 µm for the untreated films(cite Sam). Such long diffusion lengths should allow for the efficient extraction of charges in photovoltaic devices, with absorber layers which are sufficiently thick to collect most of the supra band gap solar irradiation. The combination of these optical measurements definitively shows that there is a beneficial effect of using a low concentration of ChCl as a surface treatment, in that it reduces the degree of non-radiative recombination in the film without negatively affecting the charge carrier mobility, while an increased concentration of the ChCl seems to reintroduce charge recombination pathways and effectively reduces the charge-carrier mobility.

Having shown that with the use of the compound ACN/MA solvent we are able to produce $CH_3NH_3PbBr_3$ films with increased surface coverage and improved crystallinity, and that by using a surface treatment with ChCl we are able to reduce non-radiative recombination in these films; we proceed to investigate how the films of the best quality (where the perovskite is treated with 1% ChCl) perform when incorporated into a photovoltaic device. In this work we use the n-i-p device architecture with single walled carbon nanotubes (SWNTs) interpenetrated with spiro-OMeTAD as the hole extraction layer; (FTO/SnO_2/$CH_3NH_3PbBr_3$/SWNT/spiro-OMeTAD/Au.). This architecture has previously been employed to obtain efficient mixed-cation, mixed-halide perovskite solar cells.[30] We present a schematic of the device architecture, along with the champion device results in **Figure 4**, and a cross-sectional SEM image of a typical device, along with device performance parameter statistics in **Figures S4 and S5**.

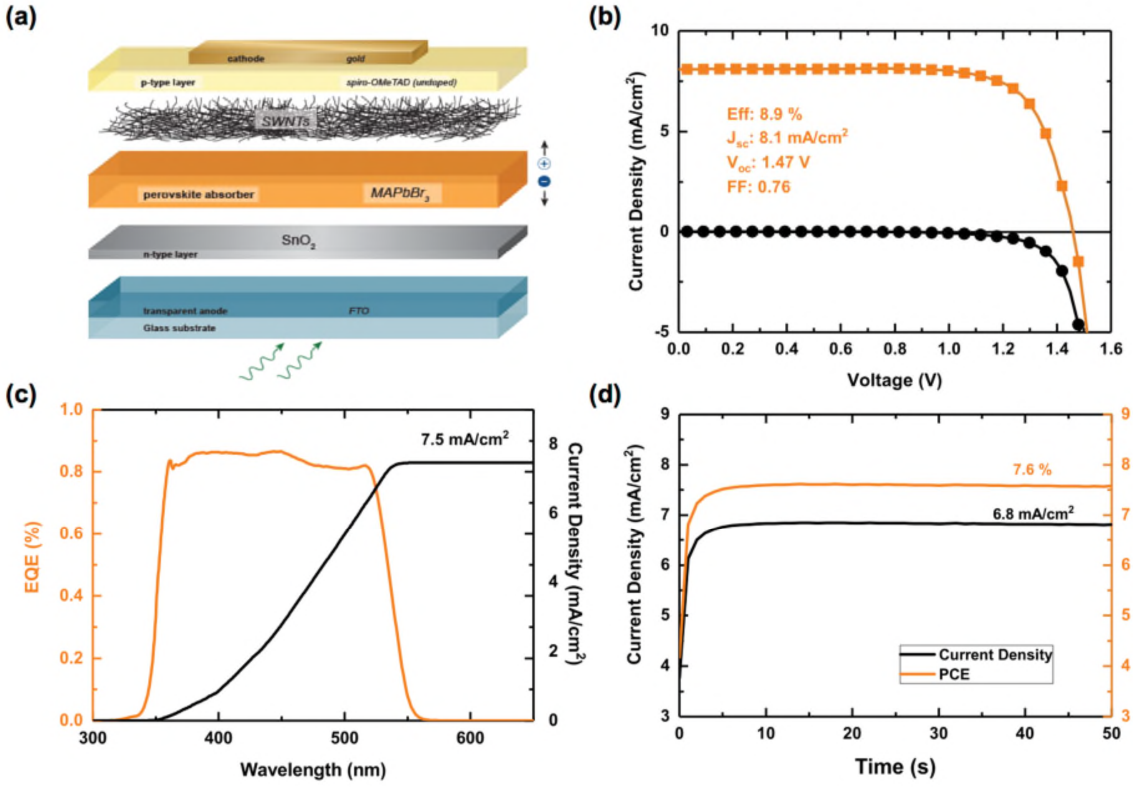

Figure 4: (a) Schematic of the device architecture employed. (b) Current-voltage curves of the champion $CH_3NH_3PbBr_3$ device. (c) External quantum efficiency (EQE) of the device shown in (b). (d) Steady state current and PCE of the champion device shown in (b).

Consistent with previous reports on $CH_3NH_3PbBr_3$ solar cells, we observe significant hysteresis in the current-voltage (JV) curves of these devices (see **Figure S6**).[21] Through the use of this compound solvent we are able to consistently obtain devices with power conversion efficiencies above 7% and achieve a maximum JV canned efficiency of 8.9%, and a steady-state efficiency of 7.6%. To corroborate the JV determined J_{sc} of 8.1 mA/cm^2, we integrate the external quantum efficiency (EQE) of this device and obtain 7.5 mA/cm^2, a value which is in close agreement. We have also been able to achieve a maximum V_{OC} of 1.52 V however, we must note that this was not achieved in the best performing device (see **Figure S7)**.

By fitting the tail of the EQE spectrum, we can determine the Urbach energy of the material. This parameter provides an estimate of the degree of electronic disorder at the band edge of the perovskite absorber material. Previous reports estimate the Urbach energy of $CH_3NH_3PbBr_3$ films at between 17 meV and 19 meV.[31] From our measurements, we determine the Urbach energies of the champion control and 1 wt.% ChCl treated devices to be 17.2 ± 0.03 meV and 16.8 ± 0.04 meV, respectively (see **Figure S8**). Additionally, we observe that if the concentration of the choline chloride used to treat the perovskite surface exceeds 1wt.%, there is a subsequent increase in the Urbach energy of the material, which corresponds to a decrease in the J_{SC} of the devices (see **Figure S9**). Typically, $CH_3NH_3PbBr_3$ devices exhibit a significant larger V_{OC} deficit, the difference in energy between the band gap of the absorber layer and the V_{OC} generated under full sun illumination, compared to their iodide-based counterparts. Chen et al. have reported voltages of up to 1.53 V for $CH_3NH_3PbBr_3$ cells fabricated using the p-i-n structure, and have suggested that the major cause of the V_{OC} limitation is not defects in the perovskite layer, but a misalignment in energy levels between the perovskite and the n-type contacts. While finding the most appropriate electron selective layers for this material is an area which is currently under investigation, the improvements in film quality gained through the deposition of these $CH_3NH_3PbBr_3$ suggests that by finding appropriate electron selective layers for this material, we should be able to further increase the performance of these devices to beyond 10%.

Conclusions:

In summary, we have demonstrated the use of the ACN/MA compound solvent system as an alternative solvent for precursor salts of the $CH_3NH_3PbBr_3$ perovskite, and shown that through the use of this solvent, we can deposit uniform, highly crystalline, wide band gap perovskite films with excellent optoelectronic properties. By using a quaternary ammonium halide salt as a passivating agent, we present a method by which we can further improve the photoluminescence lifetime and quantum efficiency of bromide-based perovskite films to a maximum of 110 ns and 5.5%, respectively. Further, we report a direct measurement of the effective charge carrier mobility of neat and passivated $CH_3NH_3PbBr_3$ films, achieving mobilities of up to 18 cm^2/Vs. By incorporating these films into photovoltaic devices, we achieve scanned power conversion efficiencies of up to 8.9%, with corresponding steady state efficiencies of up to 7.6%. Through the extension of this relatively new solvent system to the $CH_3NH_3PbBr_3$ perovskite, we have presented a scalable route to the deposition of high quality films, which when combined with an appropriate electron extraction layer, has the potential to greatly reduce the voltage losses in $CH_3NH_3PbBr_3$-based perovskite solar cells.

References:

1. M. M. Lee, J. Teuscher, T. Miyasaka, T. N. Murakami and H. J. Snaith, *Science*, 2012, **338**, 643-647.
2. H.-S. Kim, C.-R. Lee, J.-H. Im, K.-B. Lee, T. Moehl, A. Marchioro, S.-J. Moon, R. Humphry-Baker, J.-H. Yum, J. E. Moser, M. Gratzel and N.-G. Park, *Sci. Rep.*, 2012, **2**.
3. A. Kojima, K. Teshima, Y. Shirai and T. Miyasaka, *Journal of the American Chemical Society*, 2009, **131**, 6050-6051.
4. W. S. Yang, B.-W. Park, E. H. Jung, N. J. Jeon, Y. C. Kim, D. U. Lee, S. S. Shin, J. Seo, E. K. Kim, J. H. Noh and S. I. Seok, *Science*, 2017, **356**, 1376-1379.
5. D. P. W. McMeekin, Zhiping; Rahaman, Waqaas; Pulvirenti, Federico, Patel, Jay B.; Noel, Nakita K.; Marder, Seth R.; Johnston, Michael B.; Herz, Laura M.; Snaith, Henry J., *Advanced Materials*, 2017, DOI: 10.1002/(ISSN)1521-4095.
6. D. P. McMeekin, G. Sadoughi, W. Rehman, G. E. Eperon, M. Saliba, M. T. Hörantner, A. Haghighirad, N. Sakai, L. Korte, B. Rech, M. B. Johnston, L. M. Herz and H. J. Snaith, *Science*, 2016, **351**, 151-155.
7. M. Saliba, T. Matsui, J.-Y. Seo, K. Domanski, J.-P. Correa-Baena, M. K. Nazeeruddin, S. M. Zakeeruddin, W. Tress, A. Abate, A. Hagfeldt and M. Gratzel, *Energy & Environmental Science*, 2016, **9**, 1989-1997.
8. M. T. Hörantner, T. Leijtens, M. E. Ziffer, G. E. Eperon, M. G. Christoforo, M. D. McGehee and H. J. Snaith, *ACS Energy Letters*, 2017, **2**, 2506-2513.
9. C.-G. Wu, C.-H. Chiang and S. H. Chang, *Nanoscale*, 2016, **8**, 4077-4085.
10. E. Edri, S. Kirmayer, M. Kulbak, G. Hodes and D. Cahen, *The Journal of Physical Chemistry Letters*, 2014, **5**, 429-433.
11. E. Edri, S. Kirmayer, D. Cahen and G. Hodes, *The Journal of Physical Chemistry Letters*, 2013, **4**, 897-902.
12. N. K. Noel, M. Congiu, A. J. Ramadan, S. Fearn, D. P. McMeekin, J. B. Patel, M. B. Johnston, B. Wenger and H. J. Snaith, *Joule*, **1**, 328-343.
13. S. Ryu, J. H. Noh, N. J. Jeon, Y. Chan Kim, W. S. Yang, J. Seo and S. I. Seok, *Energy & Environmental Science*, 2014, **7**, 2614-2618.
14. J. H. Heo, D. H. Song and S. H. Im, *Advanced Materials*, 2014, **26**, 8179-8183.
15. S. Chen, Y. Hou, H. Chen, M. Richter, F. Guo, S. Kahmann, X. Tang, T. Stubhan, H. Zhang, N. Li, N. Gasparini, C. O. R. Quiroz, L. S. Khanzada, G. J. Matt, A. Osvet and C. J. Brabec, *Advanced Energy Materials*, 2016, **6**, 1600132-n/a.
16. G. E. Eperon, V. M. Burlakov, P. Docampo, A. Goriely and H. J. Snaith, *Advanced Functional Materials*, 2013, DOI: 10.1002/adfm.201302090, n/a-n/a.
17. M. Liu, M. B. Johnston and H. J. Snaith, *Nature*, 2013, **501**, 395-398.
18. J. Burschka, N. Pellet, S.-J. Moon, R. Humphry-Baker, P. Gao, M. K. Nazeeruddin and M. Gratzel, *Nature*, 2013, **499**, 316-319.
19. N. K. Noel, S. N. Habisreutinger, B. Wenger, M. T. Klug, M. T. Horantner, M. B. Johnston, R. J. Nicholas, D. T. Moore and H. J. Snaith, *Energy & Environmental Science*, 2017, **10**, 145-152.
20. F. C. Hanusch, E. Wiesenmayer, E. Mankel, A. Binek, P. Angloher, C. Fraunhofer, N. Giesbrecht, J. M. Feckl, W. Jaegermann, D. Johrendt, T. Bein and P. Docampo, *The Journal of Physical Chemistry Letters*, 2014, **5**, 2791-2795.
21. R. Sheng, A. Ho-Baillie, S. Huang, S. Chen, X. Wen, X. Hao and M. A. Green, *The Journal of Physical Chemistry C*, 2015, **119**, 3545-3549.
22. J. H. Noh, S. H. Im, J. H. Heo, T. N. Mandal and S. I. Seok, *Nano Letters*, 2013, **13**, 1764-1769.
23. Y. Yang, Y. Yan, M. Yang, S. Choi, K. Zhu, J. M. Luther and M. C. Beard, 2015, **6**, 7961.

24. B. Wenger, P. K. Nayak, X. Wen, S. V. Kesava, N. K. Noel and H. J. Snaith, *Nature Communications*, 2017, **8**, 590.
25. X. Zheng, B. Chen, J. Dai, Y. Fang, Y. Bai, Y. Lin, H. Wei, Xiao C. Zeng and J. Huang, 2017, **2**, 17102.
26. D. W. deQuilettes, S. Jariwala, S. Burke, M. E. Ziffer, J. T. W. Wang, H. J. Snaith and D. S. Ginger, *ACS Nano*, 2017, **11**, 11488-11496.
27. N. Kedem, M. Kulbak, T. M. Brenner, G. Hodes and D. Cahen, *Physical Chemistry Chemical Physics*, 2017, **19**, 5753-5762.
28. W. Rehman, R. L. Milot, G. E. Eperon, C. Wehrenfennig, J. L. Boland, H. J. Snaith, M. B. Johnston and L. M. Herz, *Advanced Materials*, 2015, **27**, 7938-7944.
29. W. Rehman, D. P. McMeekin, J. B. Patel, R. L. Milot, M. B. Johnston, H. J. Snaith and L. M. Herz, *Energy & Environmental Science*, 2017, **10**, 361-369.
30. S. N. Habisreutinger, B. Wenger, H. J. Snaith and R. J. Nicholas, *ACS Energy Letters*, 2017, **2**, 622-628.
31. E. T. Hoke, D. J. Slotcavage, E. R. Dohner, A. R. Bowring, H. I. Karunadasa and M. D. McGehee, *Chemical Science*, 2015, **6**, 613-617.